



**HAL**  
open science

## Measure of circularity for parts of digital boundaries and its fast computation

Tristan Roussillon, Isabelle Sivignon, Laure Tougne

► **To cite this version:**

Tristan Roussillon, Isabelle Sivignon, Laure Tougne. Measure of circularity for parts of digital boundaries and its fast computation. *Pattern Recognition*, 2010, 43 (1), pp.37-46. 10.1016/j.patcog.2009.06.014 . hal-00438631

**HAL Id: hal-00438631**

**<https://hal.science/hal-00438631v1>**

Submitted on 4 Dec 2009

**HAL** is a multi-disciplinary open access archive for the deposit and dissemination of scientific research documents, whether they are published or not. The documents may come from teaching and research institutions in France or abroad, or from public or private research centers.

L'archive ouverte pluridisciplinaire **HAL**, est destinée au dépôt et à la diffusion de documents scientifiques de niveau recherche, publiés ou non, émanant des établissements d'enseignement et de recherche français ou étrangers, des laboratoires publics ou privés.

# Measure of Circularity for Parts of Digital Boundaries and its Fast Computation <sup>★</sup>

Tristan Roussillon<sup>1</sup>

*Université de Lyon,*

*Université Lyon 2, LIRIS, UMR5205, F-69676, FRANCE*

Isabelle Sivignon

*Université de Lyon, CNRS*

*Université Lyon 1, LIRIS, UMR5205, F-69622, FRANCE*

Laure Tougne

*Université de Lyon,*

*Université Lyon 2, LIRIS, UMR5205, F-69676, FRANCE*

---

## Abstract

This paper focuses on the design of an effective method that computes the measure of circularity of a part of a digital boundary. In spite of the specificity of the digital boundaries, an algorithm that only uses classical tools of computational geometry is derived. Even if a sophisticated machinery coming from linear programming can provide a linear time algorithm, its  $\mathcal{O}(n \log n)$  time complexity is better than many quadratic methods based on Voronoi diagrams. Moreover, this bound can be improved in the case of convex digital boundaries to reach linear time.

*Key words:* circularity, compactness, digital circle, discrete geometry, computational geometry

---

## 1 Introduction

Accurately locate circles and accurately measure deviation with a circular template are common problems in many fields of science and engineering. The fields of application are as diverse as geology [1], archeology [2], computer vision such as raster-to-vector conversion [4] or video processing [5], computational metrology to test the quality of manufactured parts [6–13], image processing and discrete geometry to recognize digital circles [14–21].

This paper focuses on the design of an effective method that computes the measure of circularity of a part of a digital boundary previously extracted from a digital image. The circularity measure of a given part of a digital boundary is a quantity that increases with deviation from a piece of digital circle, called a digital arc. The reader may find in the literature terms as diverse as compactness [22,14], roundness [23,7,9–12], out-of-roundness [6,7,24], but we prefer “circularity” [25,8] because it recalls the template with which the data are compared to, that is the circle.

Although plenty of papers present methods for assessing the circularity of a set of points, as far as we know, only one paper dealt with the circularity of digital boundaries, more than twenty years ago. In [14], a digital disk recognition

---

\* Work partially supported by the GEODIB ANR project (ANR-06-BLAN-0225)  
*Email address:* `tristan.roussillon@univ-lyon2.fr` (Tristan Roussillon).

<sup>1</sup> Author supported by a grant from the DGA

19 algorithm in  $\mathcal{O}(n^2)$  is presented in the first part, and a digital compactness  
20 evaluation algorithm for digital convex objects in  $\mathcal{O}(n^3\sqrt{n})$  is presented in  
21 the second part (where  $n$  is the number of pixels of the digital boundary).  
22 The digital compactness measure is defined as the ratio between area  $A$  of the  
23 shape and area  $A'$  of the smallest enclosing digital disk (where “the smallest”  
24 is expressed in area unit, that is in number of pixels). As a smallest enclosing  
25 digital disk may not be unique and as the smallest enclosing euclidean disk  
26 may not be a smallest enclosing digital disk, areas of many digital disks have  
27 to be compared. This is why the computational cost is rather high. This first  
28 attempt shows that the problem is not trivial.

29 Moreover, naive methods that consist to find an easy-to-compute point that  
30 is expected to be the centre of a circle separating the foreground from the  
31 background are only approximative. For instance, in [26], the barycentre of  
32 a set of pixels is assumed to be the centre of a separating circle, but Fig. 1  
33 shows that if the barycentre of a set of pixels is computed, pixels that do not  
34 belong to the set may be closer to the barycentre than pixels that belong to  
35 the set, even if it turns out that the set of pixels is a digital disk.

36 A well-known circularity measure in the Euclidean plane is  $4\pi A/P^2$  where  $A$   
37 is the area and  $P$  the perimeter. The digital equivalent of this circularity mea-  
38 sure was introduced by [22], but even with a convergent perimeter estimation  
39 based on digital straight segment recognition (see [27] and [28]) the measure is  
40 theoretically unsatisfactory: digital circles may have different values that are  
41 always strictly less than 1. Moreover, this kind of measure has several other  
42 drawbacks in practice: (i) it is not perfectly scale invariant, (ii) it is not easy  
43 to interpret (iii) it is not computable on parts of a digital boundary and (iv) it  
44 is not able to provide the parameters of a circle that is close to the data. This

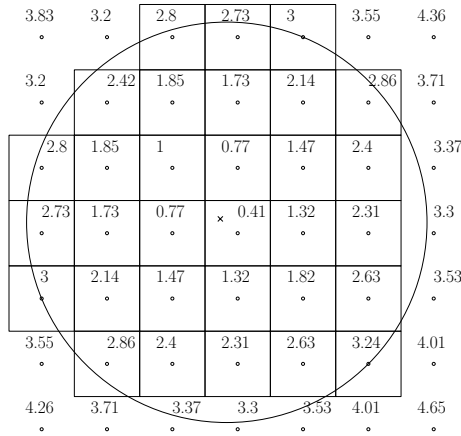


Fig. 1. A digital disk is depicted with pixels. In each pixel, the distance of its centre to the barycentre of the digital disk (located with a cross) is written. Some pixels that do not belong to the disk are closer (3.2) to the barycentre than some pixels that belong to the disk (3.24)

45 measure may be used for a coarse and quick approximation of the circularity  
 46 of a digital boundary, but in the general case, another measure is needed.

47 Three kinds of methods may be found in the literature:

48 (1) Methods based on the circular Hough transform [29–31] allow extraction,  
 49 detection and recognition of digital arcs. Even if these methods are ro-  
 50 bust against shape distortions, noise and occlusions, they require massive  
 51 computations and memory, and thresholds tuning. As the digital bound-  
 52 ary is assumed to be extracted from the digital image in this paper, the  
 53 following methods are more appropriate.

54 (2) Methods based on the separating circle problem in discrete and com-  
 55 putational geometry [15–21] allow the recognition of digital arcs. These  
 56 algorithms are not robust since one point can forbid the recognition of a  
 57 digital arc. They need to be extended to measure the extent of the deviation  
 58 with a digital arc.

59 (3) Methods based on circle fitting are widely used. In computer vision [32–  
60 34,11,4,5], a circle is fitted to a set of pixels with the least square norm.  
61 In computational metrology [6,23,7,8,24,13], a circle is fitted to a set of  
62 points sampled on the boundary of a manufactured part by a Coordinate  
63 Measurement Machine (CMM) generally with the least  $L_\infty$  norm (or  
64 Chebyshev or MinMax norm) because it is recommended by the American  
65 National Standards Institute (ANSI standard, B89.3.1-1972, R2002), but  
66 sometimes with the least square norm, like in [35].

67 In this paper, a preliminary work presented in [36] is extended. Given a part  
68 of a digital boundary, the objective is to compute a circularity measure ful-  
69 filling some properties that will be enumerated in Section ??, as well as the  
70 parameters of one separating circle if it is a digital arc or the parameters of the  
71 closest circle otherwise. The proposed method is original because it is applied  
72 on digital boundaries like the one of [14] and it links both methods based on  
73 the separating circle problem and methods based on circle fitting.

74 We formally define a circularity measure for one set of points and a pair of sets  
75 of points in Section 2. Then, we formally define a circularity measure for parts  
76 of digital boundaries in Section 3. Here is the point: from one digital boundary,  
77 two sets of points are extracted so that the circularity measure computed from  
78 these sets is representative of the circularity of the digital boundary. Thanks  
79 to this trick, in spite of the specificity of the digital boundaries, an algorithm  
80 that only uses classical tools of computational geometry is derived in Section 4.  
81 Some experiments are done on synthetic ideal, noisy digital boundaries and on  
82 real-word digital images in Section 5. The paper ends with some concluding  
83 words and future works in Section 6.

## 84 2 Circularity measure for sets of points

### 85 2.1 Cost of fitting a circle to a set of points

86 In metrology, the circularity of an arbitrary set of points  $\mathcal{S}$  in the plane is  
87 defined from the minimum cost of fitting a circle to  $\mathcal{S}$  given a certain norm.

88 The most often used norm is either  $L_2$  (least square norm) or  $L_\infty$  (MinMax or  
89 Chebyshev norm). Moreover, for both norms, the quantity that is minimized  
90 is either the sum of the radial distances or the sum of the areal distances.

91 As presented in [8], given a norm  $l$  and metric  $m$ , the cost of fitting a circle to  
92 a set of points  $S \in \mathcal{S}$  that characterizes the spread of the set of points around  
93 the circle  $\mathbf{C}$  of centre  $O$  and radius  $r$  is given by:

$$cost_{m,l}(\mathbf{C}, \mathcal{S}) = \sum_{S \in \mathcal{S}} \left\| \left| (\|\vec{OS}\|_2)^m - r^m \right| \right\|_l \quad (1)$$

94 The four instances of the problem of fitting a circle to a set of points ( $l$  equals  
95 either 2 or  $\infty$  and  $m$  equals either 1 or 2) have been thoroughly studied for a  
96 long time as it is shown in Tab. 1.

97 Notice first that the case ( $l = \infty, m = 1$ ) (also known as the measurement  
98 of Out-Of-Roundness) is recommended by the American National Standards  
99 Institute in metrology applications. Although the norm depends on the statis-  
100 tical error model, in such applications, experiments have shown that  $L_\infty$  fits  
101 provide good results ([8], for example). Moreover, the connectivity of the dig-  
102 ital boundaries, even affected by noise, guarantees that there is no outlier and  
103 that  $L_\infty$  fits may be an interesting approach in the case of digital data. Notice

m,l	2	$\infty$
1	mean square error [32,34,35]	minimum width annulus [6,23,7,8,10,11,13] ANSI standard, B89.3.1-1972 (R2002)
2	modified mean square error [33]	minimum area annulus [6,24]

Table 1

Some references for the four most used instances of the problem of fitting a circle to a set of points

104 then that for either  $l = 2$  or  $l = \infty$ , setting  $m$  to 2 is a trick that makes the  
105 computation easier because the objective function may be transformed into  
106 a problem that can be explicitly solved. As a consequence, the case ( $l = \infty$ ,  
107  $m = 2$ ) is a trade-off between accuracy ( $l = \infty$ ) and efficiency ( $m = 2$ ).

## 108 2.2 Circularity measure of a set of points

109 Given the norm  $l = \infty$  and the metric  $m = 2$ , the circularity measure of a set  
110 of points  $\mathcal{S}$  is defined from the squared radius  $r^*$  of the circle  $\mathbf{C}^*$  having the  
111 minimum cost:

$$circ(\mathcal{S}) = \frac{r^{*2} - (\text{Min}_{\mathbf{C}} \text{cost}_{2,\infty}(\mathbf{C}, \mathcal{S}))}{r^{*2} + (\text{Min}_{\mathbf{C}} \text{cost}_{2,\infty}(\mathbf{C}, \mathcal{S}))} \quad (2)$$

112 Geometrically, a circle  $\mathbf{C}$  of centre  $O$  and radius  $r$  having a cost given by  
113  $\text{cost}_{2,\infty}(\mathbf{C}, \mathcal{S})$  maps into an annulus  $\mathbf{A}$  of centre  $O$ , inner radius  $r_1$ , outer



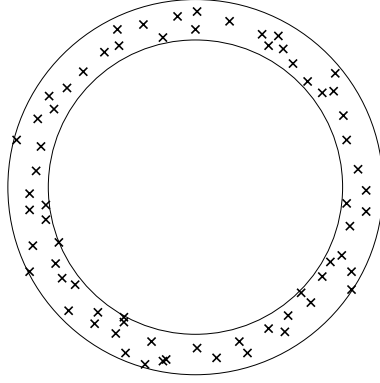


Fig. 2. Given the minimum area annulus enclosing a set of points, the circularity measure of the set of points is defined as the squared ratio between its radii.

114 radius  $r_2$  and area  $\pi(r_2^2 - r_1^2) = \pi(2 \cdot \text{cost}_{2,\infty}(\mathbf{C}, \mathcal{S}))$ . Therefore,  $\text{circ}(\mathcal{S})$  is also  
 115 the squared ratio between the radii of the minimum area annulus enclosing  $\mathcal{S}$   
 116 (Fig. 2).

117 It is clear that the measure defined by Eq. 2 is invariant to rigid transforma-  
 118 tions, equals 1 if and only if the points  $S$  of  $\mathcal{S}$  are located on one circle and is  
 119 strictly less than 1 otherwise.

### 120 2.3 Circularity measure of two sets of points

121 The goal of this subsection is to extend the previous definition of the circularity  
 122 measure of a set of points to a pair of sets of points. The interest of such an  
 123 extension will be clear in the next section.

124 Given the norm  $l = \infty$  and the metric  $m = 2$ , the cost of fitting a circle  $\mathbf{C}$   
 125 of centre  $O$  and radius  $r$  to an *inner* set of points  $\mathcal{S}$  and to an *outer* set of  
 126 points  $\mathcal{T}$  is given by:

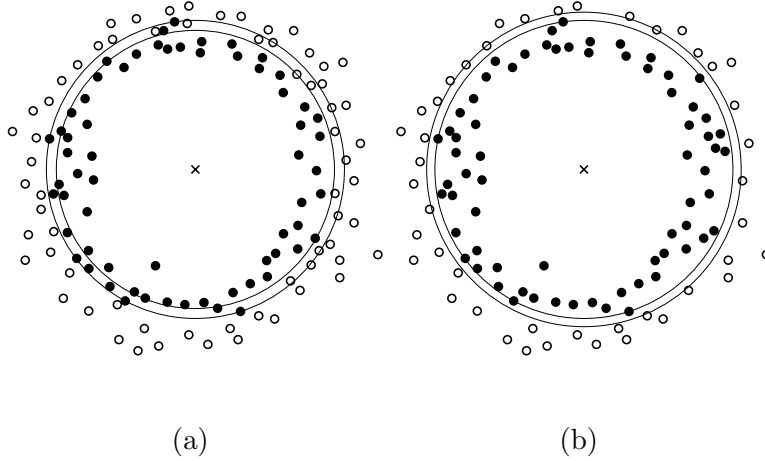


Fig. 3. Given the minimum signed area annulus enclosing a set of black disks but not the set of white disks, the circularity measure is defined as the squared ratio between its radii. The measure is greater than 1 in (a) but less than 1 in (b) because the set of black disks and the set of white disks are separable by a circle.

$$cost_{2,\infty}(\mathbf{C}, \mathcal{S}, \mathcal{T}) = \sum_{S \in \mathcal{S}} \left\| (\|\vec{OS}\|_2)^2 - r^2 \right\|_\infty + \sum_{T \in \mathcal{T}} \left\| r^2 - (\|\vec{OT}\|_2)^2 \right\|_\infty \quad (3)$$

127 The circularity measure of  $\mathcal{S}$  and  $\mathcal{T}$  is then defined as follow:

$$circ(\mathcal{S}, \mathcal{T}) = \frac{r^{*2} - (\text{Min}_{\mathbf{C}} cost_{2,\infty}(\mathbf{C}, \mathcal{S}, \mathcal{T}))}{r^{*2} + (\text{Min}_{\mathbf{C}} cost_{2,\infty}(\mathbf{C}, \mathcal{S}, \mathcal{T}))} \quad (4)$$

128 Geometrically,  $circ(\mathcal{S}, \mathcal{T})$  is also the squared ratio between the radii of the  
 129 minimum signed area annulus enclosing  $\mathcal{S}$  but not  $\mathcal{T}$  (Fig. 3).

130 **Property 1**  $circ(\mathcal{S}, \mathcal{S}) = circ(\mathcal{S})$

131 The problem of finding a minimum signed area annulus enclosing a first set  
 132 of points but not a second set of points is more general than, but may be  
 133 reduced to the usual problem of finding a minimum area annulus enclosing a

134 set of points.

135 **Property 2**  $cost_{2,\infty}(\mathbf{C}, \mathcal{S}, \mathcal{T}) \neq cost_{2,\infty}(\mathbf{C}, (\mathcal{S} \cup \mathcal{T}))$ .

136  $cost_{2,\infty}(\mathbf{C}, \mathcal{S}, \mathcal{T})$  does not characterize the spread of the two sets of points  
137 around the circle  $\mathbf{C}$  as  $cost_{2,\infty}(\mathbf{C}, (\mathcal{S} \cup \mathcal{T}))$  do, but characterizes the spread  
138 of the *penetration* of the two sets of points around the circle  $\mathbf{C}$ . Notice that  
139  $cost_{2,\infty}(\mathbf{C}, \mathcal{S}, \mathcal{T}) < 0$ , if and only if the two sets are separable by a circle  
140 (Fig. 3.b).

141 It is clear that the measure defined by Eq. 4 is invariant to rigid transforma-  
142 tions, is strictly greater than 1 if and only if  $\mathcal{S}$  and  $\mathcal{T}$  are separable by a circle  
143 and is less than 1 otherwise (Fig. 3).

144 As methods that allow the recognition of digital circles are based on the sep-  
145 arating circle problem [15–21], we have chosen to adapt the measure defined  
146 by Eq. 4 to the case of digital boundaries in the following section.

### 147 **3 Circularity measure for parts of digital boundary**

#### 148 *3.1 Data*

149 A binary image  $I$  is viewed as a subset of points of  $\mathbb{Z}^2$  that are located inside  
150 a rectangle of size  $M \times N$ . A digital object  $O \in I$  is a 4-connected subset of  $\mathbb{Z}^2$   
151 (Fig. 4.a). Note that a digital object may be defined as a 8-connected subset of  
152  $\mathbb{Z}^2$  as well. Its complementary set  $\bar{O} = I \setminus O$  is the so-called background. The  
153 digital boundary  $C$  of  $O$  is defined as the 8-connected circular list of digital  
154 points having at least one 4-neighbour in  $\bar{O}$ , (Fig. 4.b). A part  $C_{ij}$  of  $C$  is the

155 list of digital points from the  $i$ -th point to the  $j$ -th point of  $C$  (Fig. 4.c).

156 A digital disk is defined as a digital object whose points are separable from  
157 the background by an Euclidean circle (Fig. 4.d). A digital circle is defined as  
158 the boundary of a digital disk (Fig. 4.e) and a part of it is defined as a digital  
159 arc (Fig. 4.f).

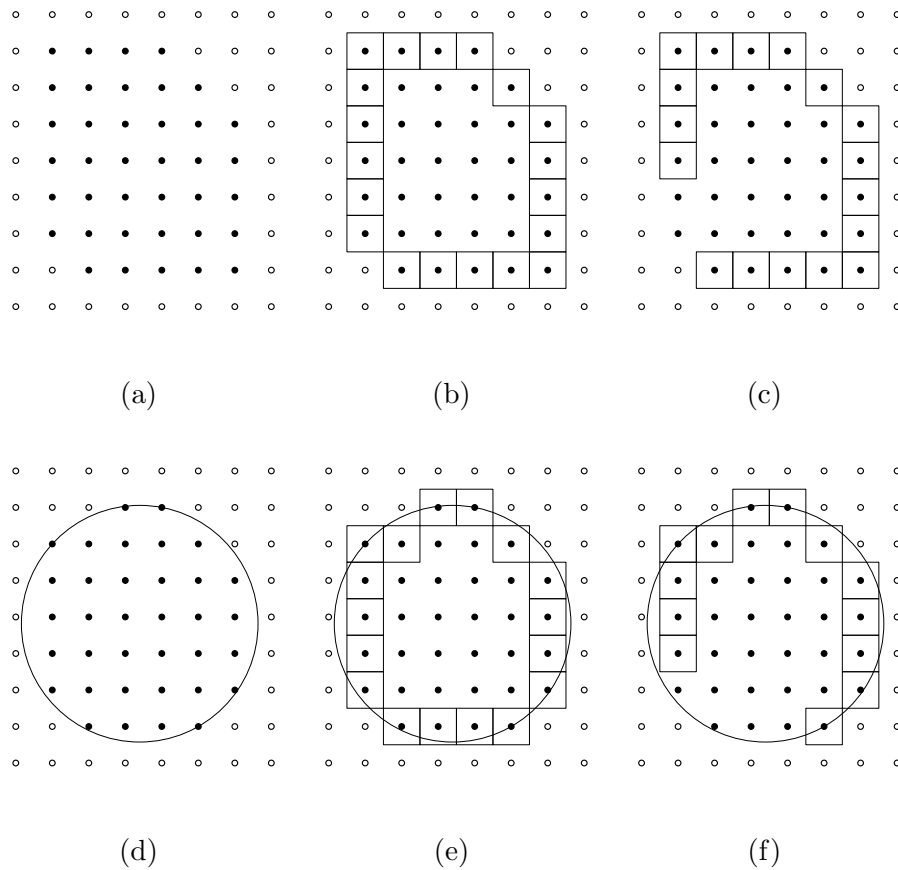


Fig. 4. (a) A digital object is depicted with black disks. The set of squares depicts the whole (b) or a part of the (c) digital boundary. (d) A digital object that is a digital disk. (e) A digital boundary that is a digital circle. (f) A part of a digital boundary that is a digital arc.

160 The goal of the two following subsections is to define a measure of how much  
161 a given part of digital boundary is far from a digital arc.

162 3.2 *Circularity measure of a part of a digital boundary*

163 A circularity measure for parts of digital boundaries is naturally expected to  
164 fulfil the following properties:

- 165 (1) be robust to translation, rotation, scaling.
- 166 (2) range from 0 to 1, equal 1 for a digital arc.
- 167 (3) be intuitive. For instance, it is naturally expected to increase as the num-  
168 ber of sides of regular polygons increases or as the eccentricity of ellipses  
169 decreases or as the amount of noise decreases. It is also expected that the  
170 measure is robust: for example, the measure of a noisy digital circle has  
171 to be higher than the measure of a digital triangle, or a digital square.

172 Fitting a circle to the points of a digital boundary does not lead to a satis-  
173 factory measure because the property 2 does not hold. However, instead of  
174 computing an annulus that encloses a set of points, we compute an annulus  
175 such that the outer disk contains all the points of the digital boundary and the  
176 inner disk does not contain any background point (Fig. 5). This is the key point  
177 of our strategy. From one digital boundary, two sets of points are extracted so  
178 that the circularity measure computed from these sets is representative of the  
179 circularity of the digital boundary.

180 Let  $\mathcal{S}$  be the set of some points of  $C$  and let  $\mathcal{T}$  be the set of some points of  
181  $\bar{O}$ . The definitions of  $\mathcal{S}$  and  $\mathcal{T}$  will be detailed in the next subsection.

182 Now, we define the circularity measure of  $C$  as the circularity measure of  $\mathcal{S}$   
183 and  $\mathcal{T}$ :

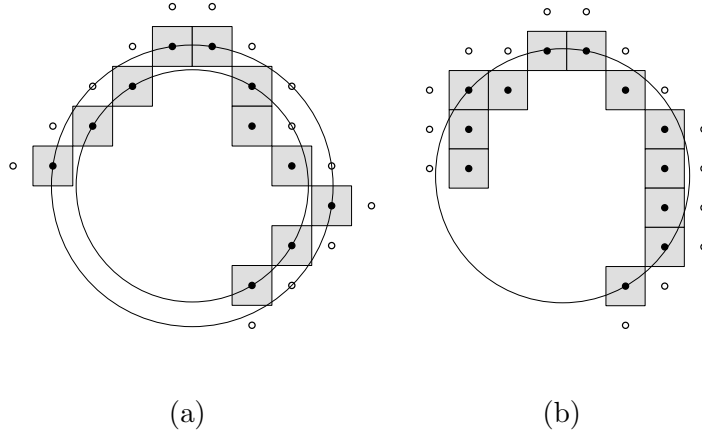


Fig. 5. Two parts of two digital boundaries are depicted with gray squares.  $\mathcal{S}$  (resp.  $\mathcal{T}$ ) is the set of black disks (resp. white disks). In (a), the minimum area annulus has an area of 4 and the circularity measure equals  $8.5/12.5 = 0.68$ . However in (b), it has a null area and the circularity measure equals 1, because the part of digital boundary is a digital arc.

$$\begin{cases} circ(C) = circ(\mathcal{S}, \mathcal{T}) & \text{if } (circ(\mathcal{S}, \mathcal{T}) < 1) \\ circ(C) = 1 & \text{otherwise} \end{cases} \quad (5)$$

### 184 3.3 Extraction of $\mathcal{S}$ and $\mathcal{T}$ from $C_{ij}$

185 Let  $C$  be a digital boundary of  $n$  digital points that is counter-clockwise ori-  
186 ented.

187 Since all circles are convex, no circle can enclose the vertices of the convex hull  
188 of  $C_{ij}$  without enclosing all its points. So  $\mathcal{S}$  may be set to the vertices of the  
189 convex hull of  $C_{ij}$ , denoted by  $\mathcal{CH}(C_{ij})$ . If  $C_{ij} \neq C$ , the first and last points  
190 of  $C_{ij}$  are put to  $\mathcal{S}$  even if they are not necessary in order to make easier the  
191 extraction of the points of  $\mathcal{T}$ .

192 Indeed, the extraction of the points of  $\mathcal{T}$  is independently performed for each  
 193 part  $C_{kl} \in C_{ij}$  that is lying between two consecutive vertices of  $\mathcal{CH}(C_{ij})$ , the  
 194 indices of which being respectively denoted by  $k$  and  $l$ .

195 As the extraction algorithm depends on the convexity of  $C_{kl}$ , the following  
 196 definition of convexity is needed:

197 **Definition 1**  $C_{ij}$  is convex (resp. concave) if there is no digital point between  
 198 the polygonal line linking the digital points of  $C_{ij}$  and the right (resp. left) part  
 199 of  $\mathcal{CH}(C_{ij})$ .

200 If  $C_{kl}$  is not convex, all the background points that are located between the  
 201 polygonal line linking the digital points of  $C_{kl}$  and the segment linking the  
 202 first and last point of  $C_{kl}$  and that are 4-neighbours of a point of  $C_{kl}$  are put  
 203 to  $\mathcal{T}$ .

204 Now we will see which background points are sufficient to add to  $\mathcal{T}$  when  $C_{kl}$   
 205 is convex.

### 206 3.3.1 Case of circles whose radius is infinite

207 Let us consider the two end points of a convex part  $C_{kl}$  that are denoted by  
 208  $s_k$  and  $s_l$ . Without loss of generality, let us consider the segment  $[s_k s_l]$  in the  
 209 forth octant, so that the background points are located above  $[s_k s_l]$ . Let us  
 210 consider the arithmetic description of  $[s_k s_l]$  with a vector  $\vec{u} = (a, b)^T$  with  
 211  $a, b \in \mathbb{Z}$  and  $\gcd(a, b) = 1$ , such that  $(s_l - s_k) = g \cdot \vec{u}$  with  $g \in \mathbb{Z}$  ( $g$  and  $\vec{u}$  may  
 212 be computed by applying Euclid's algorithm to the slope of  $[s_k s_l]$ ).

213 **Definition 2** A Bezout point  $b_q$  of a segment  $[s_k s_l]$  is defined as a point above  
 214  $[s_k s_l]$  such that  $s_k \vec{b}_q = \vec{v} + q \vec{u}$  with  $q \in \mathbb{Z}$ ,  $\vec{v} = (c, d)^T$  and  $\det(\vec{u}, \vec{v}) = 1$  ( $\vec{v}$

215 is given by the Bezout's identity that may be found thanks to the extended  
 216 Euclid's algorithm).

217 The number of Bezout points that are associated to the segment  $[s_k s_l]$  is equal  
 218 to  $g$ .

219 **Lemma 1** *A circle of infinite radius that encloses  $[s_k s_l]$  but does not enclose  
 220 any Bezout point  $b_q$ , does not enclose any other point above  $[s_k s_l]$ .*

221 This lemma and its proof may be found in other papers such as [21]. They  
 222 are the basement of the digital straight line recognition algorithm [28] because  
 223 any lower leaning point of an 8-connected digital straight segment in the first  
 224 octant that is vertically translated up by 1 is a Bezout point associated to this  
 225 segment.

226 However, it seems that only a small part of them, located near the bisector  
 227 of  $[s_k s_l]$ , are sufficient. In [21] (Definition 1), the closest point to the middle  
 228 of  $[s_k s_l]$  is arbitrarily chosen. Fig. 6 shows that only taking into account the  
 229 closest point to the middle of  $[s_k s_l]$  is not sufficient. We will see that at most  
 two Bezout points have to be taken into account.

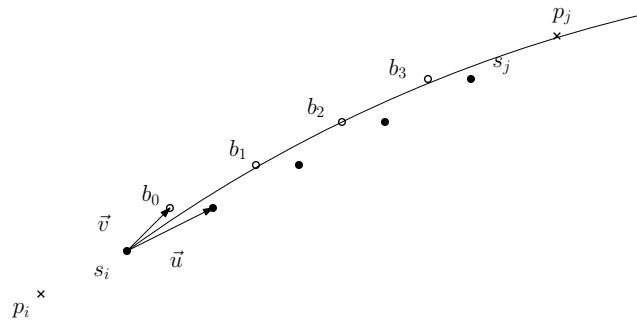


Fig. 6. This figure shows that the closest Bezout point to the middle of  $[s_k s_l]$ , denoted by  $b_1$ , is not sufficient, because there is a circle that separates  $b_1$  from  $s_k$  and  $s_l$  but encloses  $b_2$ , which is another Bezout point.

230



231 3.4 Case of circles whose radius is finite

232 For each convex part  $C_{kl}$ , let us consider two extra points defined as the  
 233 points  $p_k$  and  $p_l$  such that  $p_k = s_k - \vec{u}$  and  $p_l = s_l + \vec{u}$  (Fig. 6).  $p_k$  and  $p_l$  are  
 234 background points, since  $[s_k s_l]$  is an edge of a convex hull. The circles that  
 235 enclose  $[s_k s_l]$  but do not enclose any background point cannot have an infinite  
 236 radius because they must not enclose neither  $p_k$  nor  $p_l$ .

237 Let us introduce the following new definition:

238 **Definition 3** (Fig. 7) *The middle Bezout point(s) associated to the segment*  
 239  *$[s_k s_l]$  is(are) defined as:*

- 240 (1) *the unique Bezout point  $b_0$ , if  $g = 1$ .*
- 241 (2) *the Bezout point  $b_{g/2}$  in the special case where  $g > 1$ ,  $g$  is even and*  
 242  *$\vec{u} \cdot \vec{v} = 0$ .*
- 243 (3) *the two consecutive Bezout points  $b_q$  and  $b_{q+1}$ , such that  $q = [g/2]$  (where*  
 244  *$[.]$  is the integer part), if  $g > 1$ ,  $\vec{u} \cdot \vec{v} > 0$  or ( $\vec{u} \cdot \vec{v} = 0$  and  $g$  is odd).*

245 Then, we state the following proposition:

246 **Proposition 1** *A circle that encloses  $[s_k s_l]$  but does not enclose neither the*  
 247 *middle Bezout points associated to  $[s_k s_l]$  nor the extra points  $p_k$  and  $p_l$ , does*  
 248 *not enclose any other Bezout points.*

249 Because of its length, the proof is given in appendix, section A.

250 As a result, for each convex part  $C_{kl}$ , only two background points at most  
 251 must be kept in  $\mathcal{T}$ . Fig. 8 shows that, thanks to this arithmetic approach,  
 252 if  $C_{ij}$  is convex, the number of points of  $\mathcal{T}$  is highly reduced in comparison

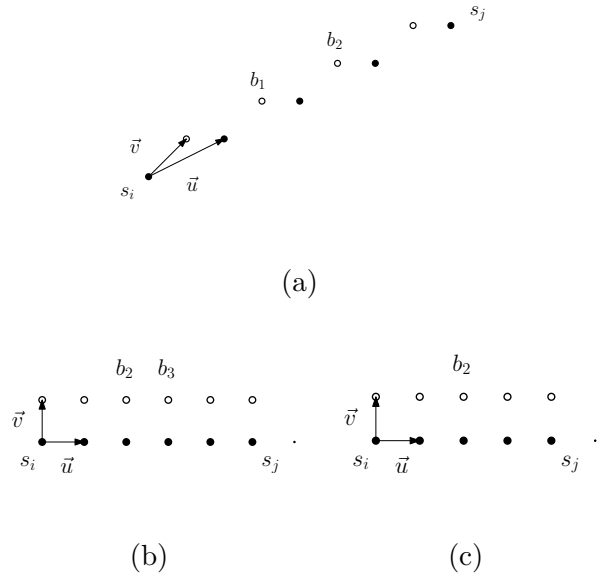


Fig. 7. (a)(b) case (3) of Def. 3 ; (c) case (2) of Def. 3.

253 to the naive approach where  $\mathcal{T}$  is the set of all background points having at  
 254 least one 4-neighbour in  $C_{ij}$ . The order of the reduction as well as the overall  
 complexity of the algorithm 1 is given below.

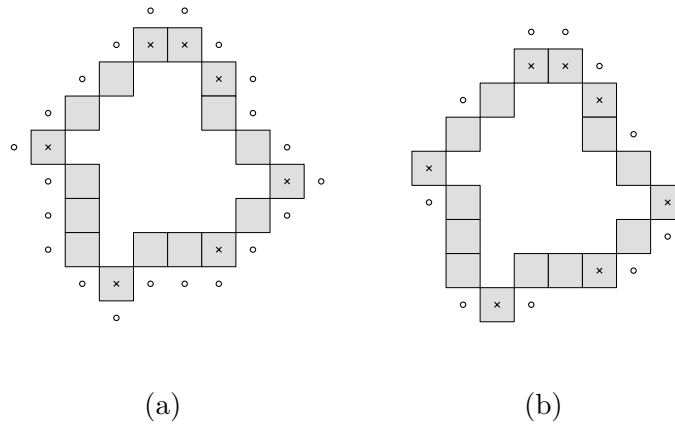


Fig. 8. Naive (a) and arithmetic (b) approach for the choice of the points of  $\mathcal{T}$   
 (white disks).

255

256 Computing  $\mathcal{CH}(C_{ij})$  (1.1) is done in linear time (using Melkman's algorithm  
 257 [44] for instance). All the background points that are 4-neighbours of a point  
 258 of  $C_{kl}$  may be computing in linear time by contour tracking. Checking whether

---

**Algorithm 1** SnTComputation( $C, \mathcal{S}, \mathcal{T}$ )

---

**Input:**  $C_{ij}$ , a part of a digital boundary**Output:**  $\mathcal{S}, \mathcal{T}$ 

- 1: Compute  $\mathcal{CH}(C_{ij})$
  - 2: **for each** part  $C_{kl}$  of  $C_{ij}$  **do**
  - 3:   Add  $s_l$  to  $\mathcal{S}$
  - 4:   **if**  $C_{kl}$  is convex **then**
  - 5:     Add the middle Bezout point(s) of  $[s_k s_l]$  to  $\mathcal{T}$
  - 6:   **else**
  - 7:     Add all the background points that are located between the polygonal line linking the digital points of  $C_{kl}$  and  $[s_k s_l]$  and that are 4-neighbours of a point of  $C_{kl}$  to  $\mathcal{T}$
  - 8: **return**  $\mathcal{S}, \mathcal{T}$
- 

259 each part  $C_{kl}$  is convex or not (1.4) and performing the appropriate processing  
260 (1.5 and 1.7) is then straightforward and also linear in time.

261 Furthermore,  $|\mathcal{S}|$  is bounded by  $\mathcal{O}(n^{2/3})$  according to known results [43]. If  
262  $C_{ij}$  is convex,  $|\mathcal{T}|$  is at most twice bigger than  $|\mathcal{S}|$  according to Proposition 1  
263 and  $|\mathcal{T}|$  is bounded by  $\mathcal{O}(n)$  otherwise. Therefore  $m = |\mathcal{S}| + |\mathcal{T}|$  is bounded  
264 by  $\mathcal{O}(n^{2/3})$  in the case of convex parts and  $\mathcal{O}(n)$  otherwise.

265 Now, we will see that  $\text{circ}(\mathcal{S}, \mathcal{T})$  is computed in  $\mathcal{O}(m \log m)$ , which leads to  
266 an algorithm that computes the circularity measure of  $C_{ij}$  in  $\mathcal{O}(n)$  if  $C_{ij}$  is  
267 convex and  $\mathcal{O}(n \log n)$  otherwise.

268 **4 Computation of  $\text{circ}(\mathcal{S}, \mathcal{T})$**

269 Let us compute the minimum area annulus  $\mathbf{A}(O, r_1, r_2)$  of centre  $O(O_x, O_y)$ ,  
 270 inner radius  $r_1$ , outer radius  $r_2$  and area  $\pi(r_2^2 - r_1^2)$ , under the following  
 271 constraints:

$$\begin{cases} \forall S \in \mathcal{S}, (S_x - O_x)^2 + (S_y - O_y)^2 \leq r_2^2 \\ \forall T \in \mathcal{T}, (T_x - O_x)^2 + (T_y - O_y)^2 > r_1^2 \end{cases} \quad (6)$$

272 *4.1 Linear programming problem*

Developing equation 6, we get:

$$\begin{cases} \forall S \in \mathcal{S}, -2aS_x - 2bS_y + f(S_x, S_y) + c_2 \leq 0 \\ \forall T \in \mathcal{T}, -2aT_x - 2bT_y + f(T_x, T_y) + c_1 > 0 \end{cases} \quad (7)$$

where  $\begin{cases} a = O_x, & b = O_y, \\ c_1 = (a^2 + b^2 - r_1^2) & c_2 = (a^2 + b^2 - r_2^2) \\ f(x, y) = x^2 + y^2 \end{cases}$

273 Instead of characterizing a circle by its centre and its radius, we characterize  
 274 a circle by its centre and the power of the origin with respect to the circle.  
 275 Thanks to this change of variables, solving (6) is equivalent to solving the  
 276 following linear program with four variables and  $|\mathcal{S}| + |\mathcal{T}|$  constraints:

PL 4D

Minimize  $d$  where  $d = (c_1 - c_2)$

subject to (8)

$$-2aS_x - 2bS_y + f(S_x, S_y) + c_2 + d \leq 0,$$

$$-2aT_x - 2bT_y + f(T_x, T_y) + c_2 > 0,$$

277 This kind of reformulation into a linear programming problem has been done,  
278 for instance, in computational geometry for the smallest enclosing circle [37]  
279 or the smallest separating circle [15], in discrete geometry for digital circle  
280 recognition [20] and in engineering for the quality control of manufactured  
281 parts [24].

282 Many techniques are known to solve such linear programming problems: for  
283 instance, the well-known simplex method, the prune and search techniques  
284 [38], the incremental randomized techniques [39]. The simplex method has a  
285 worst-case time complexity very large whereas the last two methods are linear  
286 in time in the number of points to proceed. However, these methods have some  
287 drawbacks: they are not easy to implement, they are off-line, the constant is  
288 large and is exponential in the dimension, which is equal to 4 here.

289 As an annulus is a pair of concentric circles that are characterized by three  
290 parameters each, we interpret equation 7 in a 3D space that we call *abc*-space.  
291 Indeed,  $c_1$  and  $c_2$ , having the same meaning, are both represented in the  $c$ -  
292 axis. From now, in addition to the original plane, called *xy*-plane, containing  
293 the points of  $\mathbb{Z}^2$ , we work in the *abc*-space as well as in its dual space, called

294  $xyz$ -space.

295 4.2  $abc$ -space vs  $xyz$ -space

296 As  $0 \leq r_1 \leq r_2$ ,  $a^2 + b^2 \leq c$ , the  $abc$ -space is a copy of  $\mathbb{R}^3$  from which the  
297 interior of the paraboloid of equation  $c = a^2 + b^2$  has been excluded. A point  
298 on the paraboloid maps to a circle of null radius in the  $xy$ -plane. A point that  
299 is out of the paraboloid maps to a circle whose radius is equal to the vertical  
300 distance between the point and the paraboloid in the  $xyz$ -plane (Fig. 9.a). It  
301 is clear that two points with the same projection in the  $ab$ -plane corresponds  
302 to two concentric circles in the  $xy$ -plane. Minimizing the area of an annulus  
303 bounded by such a pair of concentric circles is tantamount to minimize the  
304 vertical distance between the two corresponding points in the  $abc$ -plane.

305 However, Equation 7 involves different interpretations of the triplet  $(a, b, c)$ ,  
306 either as the coordinates of a point in the  $abc$ -space or as the coefficients  
307 of a plane in the  $xyz$ -space. In the  $xyz$ -space, all the points of  $\mathbb{Z}^2$  are lifted  
308 along an extra axis (the  $z$ -axis) according to the bivariate function  $f$ . Let  
309  $\mathcal{S}' = \{S'(S'_x, S'_y, S'_z)\}$  (resp.  $\mathcal{T}' = \{T'(T'_x, T'_y, T'_z)\}$ ) be the set of points of  
310  $\mathcal{S}$  (resp.  $\mathcal{T}$ ) that are vertically projected onto the paraboloid of equation  
311  $z = f(x, y) = x^2 + y^2$ . The  $xyz$ -space and the  $abc$ -space are dual, according to  
312 the classical definition of duality in computational geometry [40,41], that is a  
313 point in the former space maps to a plane in the latter space and conversely.  
314 Any plane in the  $xyz$ -space passing through some points of  $\mathcal{S}'$  or  $\mathcal{T}'$  cuts the  
315 paraboloid. The projection on the  $xy$ -plane of the intersection between the  
316 plane and the paraboloid is a circle that passes through the corresponding  
317 points of  $\mathcal{S}$  and  $\mathcal{T}$  (Fig. 9.b). The intersection between the paraboloid and a

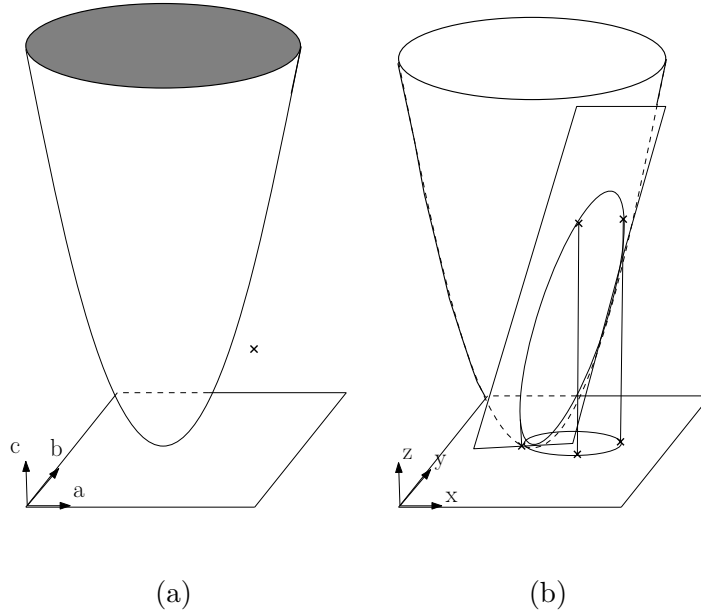


Fig. 9. (a) A point outside the paraboloid of equation  $c = a^2 + b^2$  in the  $abc$ -space corresponds to a circle in the  $xy$ -plane and conversely. (b) A plane that cuts the paraboloid of equation  $z = x^2 + y^2$  in the  $xyz$ -space corresponds to a circle in the  $xy$ -plane and conversely.

318 pair of parallel planes projects to a pair of concentric circles on the  $xy$ -plane.  
 319 Minimizing the area of an annulus bounded by such a pair of concentric circles  
 320 is tantamount to minimize the vertical distance between the two correspond-  
 321 ing planes in the  $xyz$ -plane. This kind of transformation is well known in  
 322 computational geometry [40,41] and has already been used in [37] to solve the  
 323 smallest enclosing circle or in [15,20] to solve the separating circle problem.

324 The understanding of the constraints is more straightforward in the  $xyz$ -plane  
 325 and that is why we will preferably work in this space in the following subsec-  
 326 tion.

327 4.3 Pair of parallel planes

328 We have to compute a pair of parallel planes such that the upper plane is  
329 above the points of  $\mathcal{S}'$  and the lower plane is below the points of  $\mathcal{T}'$  in order  
330 to solve equation 7 and derive a circularity measure.

331 Obviously,  $\mathcal{S}'$  and  $\mathcal{T}'$  may be reduced to their convex hull denoted by  $CH(\mathcal{S}')$   
332 and  $CH(\mathcal{T}')$ . In addition, the property of convexity makes the next step that  
333 consists in minimizing the vertical distance between the two parallel planes of  
334 support more efficient.

335 We do not detail the classical convex hull computation algorithm that may  
336 run in  $\mathcal{O}(m \log m)$ , where  $m = |\mathcal{S}'| + |\mathcal{T}'|$  [40,41].

337 An elementary way to compute the pair of parallel planes of support minimiz-  
338 ing their vertical distance is to compute the intersection depth between the two  
339 polyhedra  $CH(\mathcal{S}')$  and  $CH(\mathcal{T}')$  denoted by  $h = \min Height(CH(\mathcal{S}'), CH(\mathcal{T}'))$ .  
340  $Height(CH(\mathcal{S}'), CH(\mathcal{T}'))$  is a function that returns the distance between the  
341 two polyhedra computed along the  $z$ -axis for each point of the domain of the  
342 function. Notice that  $Height(CH(\mathcal{S}'), CH(\mathcal{T}'))$  is not defined everywhere. In-  
343 deed, the domain of this function is the intersection of the projection on the  
344  $xy$ -plane of  $CH(\mathcal{S}')$  and  $CH(\mathcal{T}')$ , that is  $CH(\mathcal{S}) \cap CH(\mathcal{T})$ .

345 To compute  $h$ , the brute force algorithm consists in computing the planar  
346 graph  $G^*$  that is the intersection between  $G_{\mathcal{S}}$  and  $G_{\mathcal{T}}$  (Fig. 10). If  $|G^*| = 0$ ,  
347 then  $CH(\mathcal{S}) \cap CH(\mathcal{T}) = \emptyset$ . In this degenerate case,  $\mathcal{S}'$  and  $\mathcal{T}'$  are separable by  
348 a plane that is orthogonal to the  $xy$ -plane,  $\mathcal{S}$  and  $\mathcal{T}$  are separable by a circle  
349 of infinite radius, that is a straight line, so the part of digital boundary from



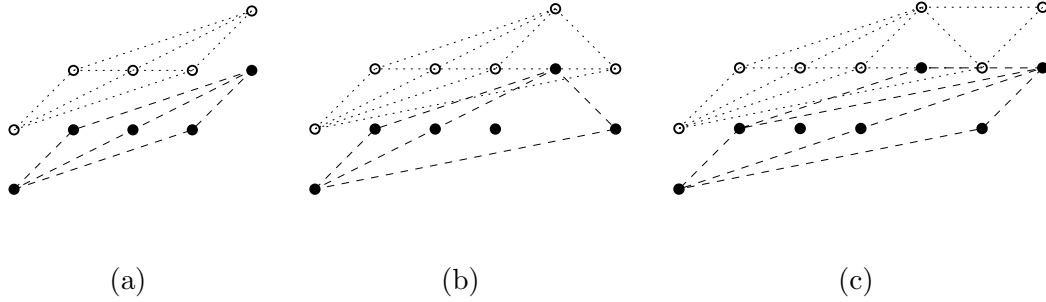


Fig. 10.  $\mathcal{S}$  (black disks) and  $\mathcal{T}$  (white disks) are separable by straight line in (a) by a circle in (b) and are not separable by a circle in (c). Note that  $G^*$ , which is the intersection between  $G_{\mathcal{S}}$  (in dashed lines) and  $G_{\mathcal{T}}$  (in dotted lines), has respectively 0, 4 and 3 nodes in (a), (b) and (c).

350 which  $\mathcal{S}$  and  $\mathcal{T}$  have been computed is a digital straight segment (Fig. 10.a).  
 351 If  $|G^*| > 0$ , it remains to compute the height function for each vertex of  $G^*$   
 352 and take the minimum.

353 The brute force algorithm runs in  $\mathcal{O}(m^2)$  since  $G^*$  has at most  $m^2$  vertices.  
 354 However, it is possible to take advantage of the convexity of the height function  
 355 to get an algorithm in  $\mathcal{O}(m \log m)$  (see [40, pages 310-315] for this algorithm).

356 Since  $h$  is the signed area of the annulus  $\mathbf{A}$ , if  $h \leq 0$ ,  $\mathcal{S}$  and  $\mathcal{T}$  are separable  
 357 by a circle and  $\text{circ}(\mathcal{S}, \mathcal{T}) = 1$  but if  $h > 0$ ,  $\mathcal{S}$  and  $\mathcal{T}$  are not separable by a  
 358 circle and  $\text{circ}(\mathcal{S}, \mathcal{T}) = \frac{r_1^2}{r_2^2}$ , where  $r_1^2$  and  $r_2^2$  are derived from the coefficients  
 359 of the pair of parallel planes.

360 Although our algorithm is more general than a simple digital circle test, its  
 361 complexity in  $\mathcal{O}(m \log m)$  is better than the quadratic complexity of the meth-  
 362 ods presented in [16,17,21]. These methods cannot be efficient because they  
 363 only deal with 2D projections of 3D polyhedrons.

364 Algorithm 2 sums up the current section.

---

**Algorithm 2** *CircularityComputation*( $\mathcal{S}, \mathcal{T}$ )

---

**Input:**  $\mathcal{S}$  and  $\mathcal{T}$ , two sets of points

**Output:** *circ*( $\mathcal{S}, \mathcal{T}$ )

- 1: Compute  $\mathcal{S}'$  and  $\mathcal{T}'$  from  $\mathcal{S}$  and  $\mathcal{T}$
  - 2: Compute  $CH(\mathcal{S}')$  and  $CH(\mathcal{T}')$
  - 3: Compute the pair of parallel planes of support
  - 4: Derive  $r_1$  and  $r_2$  from the coefficients of the planes
  - 5: **if**  $r_1 \leq r_2$  **then**
  - 6:     **return**  $r_1^2/r_2^2$
  - 7: **else**
  - 8:     **return** 1
- 

## 365 5 Experiments

366 By definition, the circularity measure that is proposed in Section ?? is on the  
367 one hand invariant under similarity transformations and on the other hand  
368 maximum and equal to 1 for any digital circle whatever its centre or its radius.  
369 In this section the behaviour of the measure is probed with respect to either  
370 synthetic images or real-world images.

### 371 5.1 Synthetic images

372 The measure is computed on different classes of objects, either noise-free ob-  
373 jects that are not circles, such as ellipses and regular polygons or noisy circles  
374 (Fig. 11) and compared with the ground truth, which is computed from the  
375 smallest area annulus enclosing the continuous objects.

376 First, one hundred digital polygons were generated (Gauss digitization of reg-


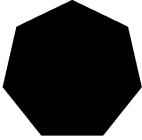


			
ellipse	regular 7-gon	noisy disk	noisy disk
$a = 25, b = 50$	$p = 1325$	$r = 30, \alpha = 1$	$r = 30, \alpha = 15$

Fig. 11. Gauss digitization of an ellipse, a regular 7-gon and two disks. The visual size of the shapes does not reflect their true size. The amount of noise that is added to the two latter shapes according to the degradation model of [46] depends of parameter alpha (Eq 9). The digital curves that we are called upon to measure are the 8-connected boundaries of these digital objects.

ular polygons of fixed perimeter). Their number of sides is ranging from 3 to  
 103, whereas their perimeter  $p$  is approximately equal to 1325 (pixels). A  
 so large perimeter enables to observe light variations of circularity within a  
 wide range of number of sides. Fig. 12 shows that the measure is close to the  
 ground truth. As expected, the circularity increases with the number of sides  
 and converges towards 1. The bigger the number of sides, the more the poly-  
 gons look like a circle and the more the circularity is close to 1. Note that the  
 circularity of the  $k$ -gons where  $30 \leq k < 85$  is alternatively equal to 1 and to a  
 value that is slightly less than 1, namely approximately 0.99. Furthermore, the  
 $k$ -gons where  $k \geq 85$  are digitized into a same digital object whose circularity  
 is 1.

Next, hundreds of digital ellipses (Gaussian digitization of continuous ellipses)  
 were generated with various parameters :  $a$  (resp.  $b$ ), small (resp. great) semi-  
 axis,  $\theta$ , the angle between the main axis of the ellipse and the  $x$ -coordinate

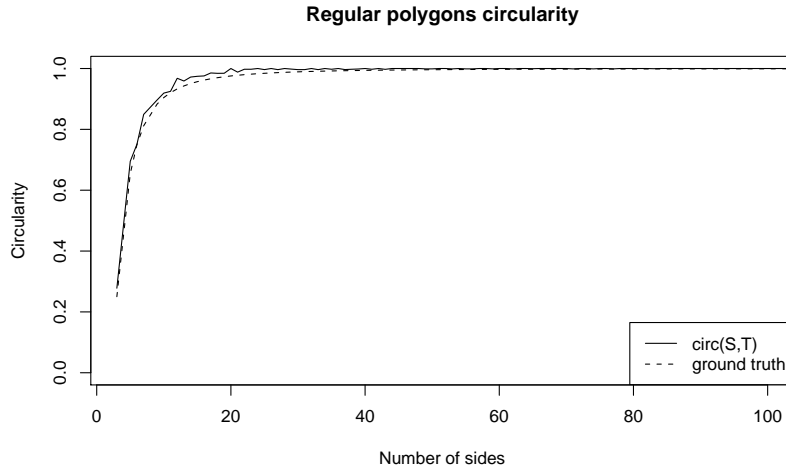


Fig. 12. One hundred regular polygons of perimeter approximately equal to 1325. Circularity is plotted against the number of sides.

391 axis,  $O_x$  and  $O_y$  the coordinates of the ellipse centre. Fig. 13 shows that the  
 392 measure behaves very well and is nearly confounded to the ground truth.

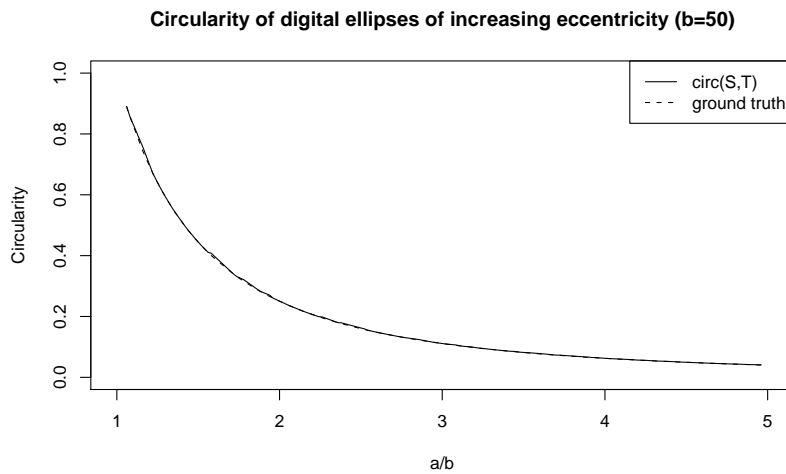


Fig. 13. One hundred of digital ellipses were generated according to the following rules:  $O(0,0)$ ,  $\theta = 0$ ,  $b = 50$  and  $a$  is ranging from 10 to 50. Circularity is plotted against  $a/b$ , the eccentricity of the ellipses.

393 Finally, hundreds of noisy circles are generated. In order to study the im-  
 394 pact of the amount of noise onto circularity, we implemented a degradation

395 model very close to the one investigated in [46]. This model was proposed  
 396 and validated in the context of document analysis and assume that: (i) the  
 397 probability to flip a pixel (that is, label ‘foreground’ or ‘1’ a pixel previously  
 398 labelled ‘background’ or ‘0’, and conversely) depends of its distance to the  
 399 nearest pixel of the complement set and (ii) blurring may be simulated with  
 400 a morphological closing. Thus, in practice:

- 401 • we perform a squared Euclidean distance transform [47];
- 402 • we process each pixel according to formula 9, which is a simplified version  
 403 of only one parameter of the model investigated in [46]:

$$p(0|1)_{P_{ij}} = p(1|0)_{P_{ij}} = \exp\left(-\frac{SEDT(P_{ij})}{\alpha}\right) \quad (9)$$

404 where  $SEDT(P_{ij})$  is the squared Euclidean distance that is stored at pixel  
 405  $P_{ij}$  in the distance map and  $\alpha$  is a parameter that controls the amount of  
 406 noise;

- 407 • we apply a morphological closing with a circular structuring element whose  
 408 radius is 5, which makes the object connected again.

409 Figure 11 gives two examples of results of the degradation algorithm applied to  
 410 a digital disk. Figure 14 shows that the circularity decreases with the amount of  
 411 noise, but with sawtooth because the pixels are flipped at random. The noisier  
 412 the digital circle, the more it looks different from a digital circle. Furthermore,  
 413 even with rather noisy digital circles ( $\alpha = 15$ ), the circularity is above 0.8,  
 414 which approximately corresponds to the circularity of a 7-gon. Hence, the  
 415 measure is sufficiently robust to discriminate noisy circles given by the noise  
 416 model of [46] at  $\alpha = 15$ , from  $k$ -gons where  $k < 7$ , such as squares or triangles.  
 417 Note that the comparison makes sens in spite of the difference of perimeter

418 because the measure is size invariant.

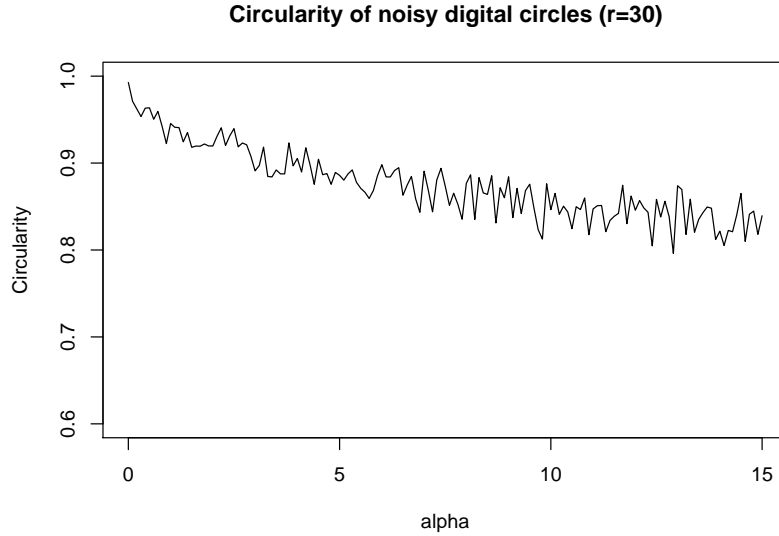


Fig. 14. One hundred digital circles of radius 30 are generated with more and more noise. Parameter alpha ranging from 1 to 15 controls the amount of noise (Fig. 11). Circularity is plotted against parameter alpha.

419 The accuracy of the measurements on digital arcs of various length is now  
420 investigated. Fifty noisy circles are generated ( $r = 30, \alpha = 15$ ) (Fig. 11).  
421 For each circle and for each length from 20 to approximately 180 pixels, one  
422 digital arc is randomly extracted. The circularity measure is computed from  
423 these approximately 7500 digital arcs. Fig. 15 shows that from 20 to 45 pixels  
424 of length (90 degrees), measurements are not accurate, because the confidence  
425 range at 95% is wide (until more than 0.1). Though, the confidence range  
426 shrinks while the arc length increases and the measurements done on digital  
427 arcs of more than 45 pixels of length (90 degrees) may be consider accurate.  
428 Obviously, the smallest angle for which measurements are accurate depends  
429 on the noise and the size of the digital circles. The smaller  $\alpha$  is, the smaller  
430 the angle is. In the special case where  $\alpha = 0$ , measurements are perfect for  
431 all digital arcs. Moreover, the higher the radius is, the less the noise added by

432 the model at a given  $\alpha$  affects the shape, the smaller the angle is.

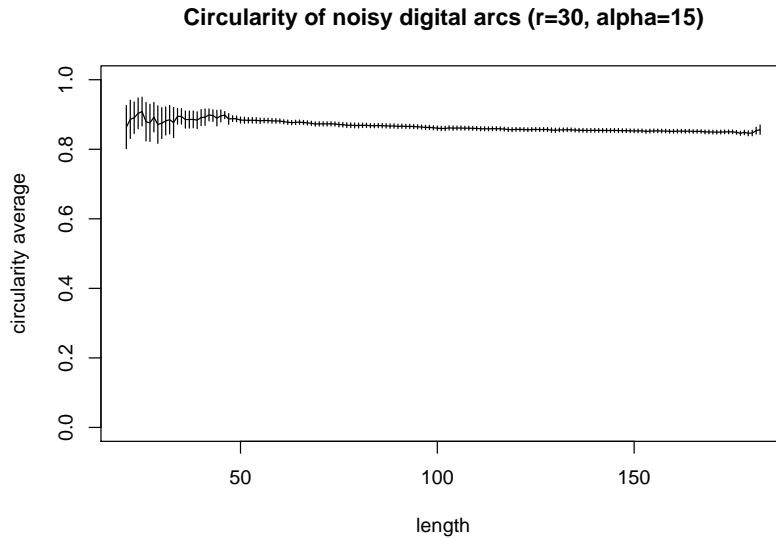


Fig. 15. Fifty noisy circles were generated ( $r = 30$ ,  $\alpha = 15$ ) (Fig. 11). For each circle, for each length from 20 to approximately 180 pixels, one digital arc is randomly extracted. The average of the circularity measure of the digital arcs (solid line) is plotted against the length with error bars at 95%.

## 433 5.2 Real-world images

434 We are currently working in collaboration with geographers. They want to  
435 perform a set of measurements that describes the shape of pebbles sedimented  
436 in river beds. The underlying assumption is that pebbles size and shape are  
437 determined by lithology, distance of transport, abrasion, etc. The objective is  
438 to reduce the subjectivity and the time spent in the field thanks to digital  
439 image analysis.

440 The circularity measure proposed in this paper is used in order to study the  
441 shape of pebbles from digital images, collected in the bed of the Progo, an  
442 Indonesian river located on Java Island near Yogyakarta. Approximately 1300

443 pebbles were randomly sampled in the bed, with 2 photos being taken on 12  
444 stations located at various distances from the source. Fig. 16 shows two photos  
taken near the source.



445 Fig. 16. Zoom in photos taken on the first (left) and second (right) stations.

446 First, we detected pebbles with clustering methods in the HSV (hue, saturation,  
447 value) color-space. Next, we extracted the digital curves that bound each  
448 pebble by contour tracking. Finally, the circularity measure was computed for  
449 all the digital curves.

450 In Fig. 17, the average of the circularity measure of the pebbles is plotted  
451 against the distance from the source of the stations where the pebbles have  
452 been collected. Circularity is valuable for geographers because experiments  
453 shows that it increases in the first 20 kilometres, while the pebbles get rounder  
454 (like a roundness index [1]), but has a complex pattern after, with no clear  
455 trend, which raises the possibility of a substitution of macro-scale to micro-  
456 scale shape changes downstream. Note that Fig. 16 shows photos taken on  
457 two stations that have statistically significant difference of circularity: the first  
458 station (Fig. 16, left) and the second one (Fig. 16, right). Obviously, other size,  
459 form and shape parameters, like diameter, elongation, convexity and various  
460 roundness indices, add to circularity to provide multidimensional data of great



interest for geographers.

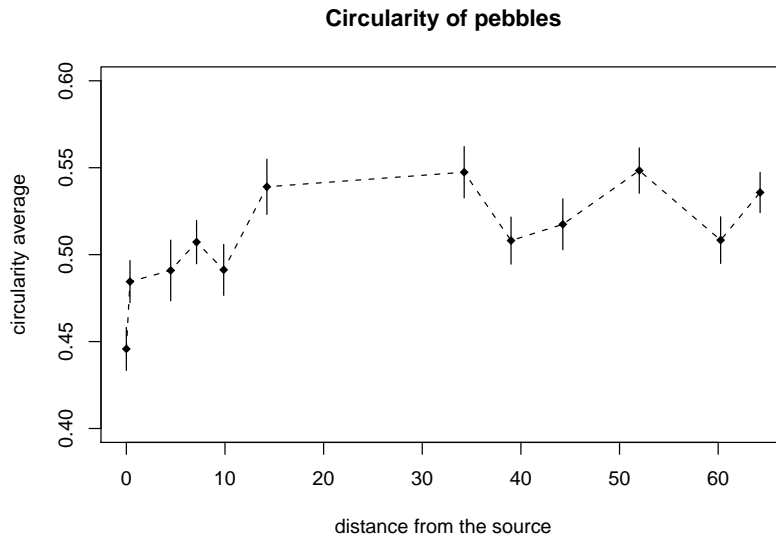


Fig. 17. The average of the circularity measure of the pebbles is plotted against the distance from the source of the 12 stations where the 1300 pebbles have been collected.

461

462 In the left photo of Fig. 16, two pebbles are badly detected because they touch  
463 each other. In such a case, it is possible to cut the digital curve in two, thanks  
464 to an algorithm that robustly decomposes a digital curve into convex and  
465 concave parts [48], and independently deal with the two open digital curves.  
466 As the missing part is very small, the circularity measure is very close to the  
467 one that could have been computed on the unknown closed digital curve.

## 468 6 Conclusion and perspectives

469 In this paper, a circularity measure has been defined for parts of digital bound-  
470 aries. An existing circularity measure of a set of discrete points (Section 2.2),  
471 which is sometimes used in computational metrology, is extended to the case

472 of a pair of sets of discrete points (Section 2.3) and then to the case of parts of  
473 digital boundaries (Section 3.2). Once the minimum area annulus, such that  
474 the outer disk contains all the points of the part of a digital boundary and the  
475 inner disk does not contain any background point is computed, the circular-  
476 ity measure is defined as the squared ratio between the inner and outer radii  
477 (Section 3.2).

478 Because we consider two sets of points, the problem we deal with is more  
479 general than the usual problem of finding a minimum area annulus enclosing  
480 one set of points [6,23,7,8,10,11,13]. The circularity measure of these two sets  
481 of points is computed thanks to an algorithm in  $\mathcal{O}(n \log n)$  that only uses  
482 classical tools of computational geometry (Section 4.3). The method is exact  
483 contrary to many methods that use *ad hoc* heuristics [8] or meta-heuristics  
484 like simulated annealing [11,13]. Even if it is shown that a sophisticated ma-  
485 chinery coming from linear programming can provide a linear time algorithm  
486 (Section 4.1), its  $\mathcal{O}(n \log n)$  time complexity is better than many methods  
487 based on Voronoi diagrams [16,17,6,23] (Section 4.3). Moreover, the two sets  
488 (points of the digital boundary and background points) are cull so that the  
489 complexity reach linear time in the case of convex digital boundaries (Sec-  
490 tion 3.3).

491 The measure fulfils the following properties:

- 492 • it may be applied on digital boundaries or any part of it.
- 493 • it is robust to rigid transformations.
- 494 • it increases as the number of sides of a regular polygon increases (Fig. 12),  
495 as eccentricity decreases (Fig. 13), and as noise decreases (Fig. 14).
- 496 • it ranges from 0 to 1 and is equal to 1 for any digital circle or arc.

497 • it provides the parameters of a circle whose digitization is the measured  
498 part of digital boundary if the circularity measure is 1 and the parameters  
499 of an approximating circle otherwise.

500 The kind of measure and algorithm proposed in this paper is general enough to  
501 be applied in order to recognize or measure the deviation with other quadratic  
502 shapes like parabolas. In the case of parabolas, the extension is straightfor-  
503 ward: it is enough to modify function  $f$ , so that  $f(x, y)$  equals  $x^2$  (or  $y^2$ ),  
504 instead of  $x^2 + y^2$ . The points of the  $xy$ -plane are merely vertically projected  
505 onto a parabolic cylinder instead of an elliptic paraboloid and algorithm 2 does  
506 not change. Obviously, algorithm 1 must be modified, because it is optimised  
507 for circles. Adopting a naive approach, a new one may be easily sketched.

508 To end, it would be quite valuable to make the algorithm on-line (without  
509 increasing its complexity as far as possible). The on-line property would be  
510 of great interest to efficiently and robustly decompose a digital boundary into  
511 primitives like digital arcs or pieces of digital parabolas.

## 512 **A Proof of Proposition 1**

513 In the sequel, we only consider the case of a circle that encloses  $[s_k, s_l]$  but nei-  
514 ther  $p_l$  nor the closest middle Bezout point to  $p_l$ . The other case is symmetric  
515 and the two cases will be put together to conclude the proof.

516 Let us consider a circle passing through  $s_k$  and  $p_l$ . If such a circle encloses  $s_l$   
517 but does not enclose any Bezout point, then any circle passing through  $s_k$  and  
518 intersecting  $[s_l, p_l]$  (of whatever radius) separates  $s_l$  from any Bezout point too.

519 The first point  $b$  that is touched by a circle passing through  $s_k$  and  $p_l$  of  
 520 decreasing radius is such that the angle between  $\vec{bs}_k$  and  $\vec{bp}_l$  is maximized. To  
 521 maximize such an angle in the range  $[\pi/2, \pi]$  is equivalent to maximize the  
 522 tangent of the angle that equals:

$$\frac{\det(\vec{bs}_k, \vec{bp}_l)}{\vec{bs}_k \cdot \vec{bp}_l}$$

523 However,  $\det(\vec{bs}_k, \vec{bp}_l)$  is constant and equal to  $g + 1 = h$ . Then, only taking  
 524 into account the denominator, we look for the integer  $q$  that minimizes:

$$f : \mathbb{Z} \mapsto \mathbb{Z}$$

$$f(q) = (-\vec{v} - q\vec{u}) \cdot (-\vec{v} + (h - q)\vec{u})$$

525 Developing, we finally get:

$$f(q) = q^2(\|\vec{u}\|^2) + q(2(\vec{u} \cdot \vec{v}) - h(\|\vec{u}\|^2)) + (\|\vec{v}\|^2 - h(\vec{u} \cdot \vec{v}))$$

526 The derivative is:

$$f'(q) = (2\|\vec{u}\|^2)q + 2(\vec{u} \cdot \vec{v}) - h(\|\vec{u}\|^2)$$

527 Since  $2\|\vec{u}\|^2 \geq 0$ ,  $f$  is convex and has a global minimum at the value of  $q$  for  
 528 which  $f'(q)$  is closer to 0 than for the other values of  $q$ . The minimum seems  
 529 to be reached around  $q = h/2$  because  $f'(h/2) = 2(\vec{u} \cdot \vec{v}) \geq 0$ . Since  $q$  has  
 530 to be an integer, the parity of  $h$  involves two different cases that need to be  
 531 independently discussed.

532 Let us consider that  $h$  is even. We show that  $q$  equals  $h/2$  because  $f(h/2) \leq$   
533  $f(h/2 + 1)$ ,  $f(h/2) \leq f(h/2 - 1)$ . Indeed,  $f'(h/2 + 1) = 2\|\vec{u}\|^2 + 2(\vec{u} \cdot \vec{v})$ , which  
534 is positive and greater than  $2(\vec{u} \cdot \vec{v})$ . Similarly,  $f'(h/2 - 1) = -2\|\vec{u}\|^2 + 2(\vec{u} \cdot \vec{v})$ .  
535 Now,  $2\|\vec{u}\|^2 - 2(\vec{u} \cdot \vec{v}) > 2(\vec{u} \cdot \vec{v}) \Leftrightarrow \|\vec{u}\|^2 > 2(\vec{u} \cdot \vec{v})$ . That equation being always  
536 true, we can conclude that  $q$  equals  $h/2$ .

537 Let us consider that  $h$  is odd. It is clear that the minimum is reached at  
538  $h/2 - 1/2$  or  $h/2 + 1/2$ . On the one hand,  $f'(h/2 + 1/2) = \|\vec{u}\|^2 + 2(\vec{u} \cdot \vec{v})$  and  
539 on the other hand,  $f'(h/2 - 1/2) = -\|\vec{u}\|^2 + 2(\vec{u} \cdot \vec{v})$ . If  $\vec{u} \cdot \vec{v} = 0$ , the minimum  
540 is reached at both  $h/2 - 1/2$  and  $h/2 + 1/2$ , but if  $\vec{u} \cdot \vec{v} > 0$ , it is clear that the  
541 minimum is only reached at  $h/2 - 1/2$ .

542 Finally, the first point  $b$  that is touched by the circle of decreasing radius and  
543 passing through  $s_k$  and  $p_l$  is the closest middle Bezout point to  $p_l$  according to  
544 Def. 3. Tab. A.1 summarizes the previous results whereas Tab. A.2 gives the  
545 results of the symmetric case. Merging the two tables, the three cases of Def. 3  
546 appear and this concludes the proof of Proposition 1. The last two items of  
Def. 3 are illustrated in Fig. 7.  $\square$

$\vec{u} \cdot \vec{v}$	$h$	$g$	$q$	Def. 3	Fig. 7
$\geq 0$	even	odd	$h/2 = g/2 + 1/2 = [g/2] + 1$	(3)	(b)
0	odd	even	$h/2 - 1/2 = g/2 = [g/2]$ $h/2 + 1/2 = g/2 + 1 = [g/2] + 1$	(2)	(c)
$> 0$	odd	even	$h/2 - 1/2 = g/2 = [g/2]$	(3)	(a)

Table A.1

Results for the case of a circle that encloses  $[s_k s_l]$  but neither  $p_l$  nor the middle  
Bezout point the closest to  $p_l$  (with  $g > 1$ ).

$\vec{u} \cdot \vec{v}$	$h$	$g$	$q$	Def. 3	Fig. 7
$\geq 0$	even	odd	$h/2 - 1 = g/2 - 1/2 = [g/2]$	(3)	(b)
0	odd	even	$h/2 - 1/2 - 1 = g/2 - 1 = [g/2] - 1$ $h/2 + 1/2 - 1 = g/2 = [g/2]$	(2)	(c)
$> 0$	odd	even	$h/2 - 1/2 - 1 = g/2 - 1 = [g/2] - 1$	(3)	(a)

Table A.2

Results for the symmetric case of a circle that encloses  $[s_k s_l]$  but neither  $p_k$  nor the middle Bezout point the closest to  $p_k$  (with  $g > 1$ ).

547

## References

- [1] H. Wadell, Volume, shape, and roundness of rock particles, *Journal of Geology* 40 (1932) 443–451.
- [2] A. Thom, A statistical examination of megalithic sites in britain, *Journal of Royal Statistical Society* 118 (1955) 275–295.
- [3] V. Karimaki, Effective circle fitting for particle trajectories, *Nuclear Instruments and Methods in Physics Research, Section A* 305 (1991) 187–191.
- [4] X. Hilaire, K. Tombre, Robust and accurate vectorization of line drawings, *IEEE Transactions on Pattern Analysis and Machine Intelligence* 28 (6) (2006) 890–904.
- [5] I. Frosio, N. A. Borghese, Real-time accurate circle fitting with occlusions, *Pattern Recognition* 41 (2008) 1045–1055.
- [6] V.-B. Le, D. T. Lee, Out-of-roundness problem revisited, *IEEE Transactions on Pattern Analysis and Machine Intelligence* 13 (3) (1991) 217–223.

- [7] K. Swanson, D. T. Lee, V. L. Wu, An optimal algorithm for roundness determination on convex polygons, *Computational Geometry* 5 (1995) 225–235.
- [8] J. Pegna, C. Guo, Computational metrology of the circle, in: *Computer graphics international*, 1998, pp. 350–363.
- [9] M. de Berg, P. Bose, D. Bremner, S. Ramaswami, G. Wilfong, Computing constrained minimum-width annuli of points sets, *Computers-Aided Design* 30 (4) (1998) 267–275.
- [10] P. K. Agarwal, B. Aronov, S. Har-Peled, M. Sharir, Approximation and exact algorithms for minimum-width annuli and shells, *Discrete & Computational Geometry* 24 (4) (2000) 687–705.
- [11] M.-C. Chen, Roundness measurements for discontinuous perimeters via machine visions, *Computers in Industry* 47 (2002) 185–197.
- [12] P. Bose, P. Morin, Testing the quality of manufactured disks and balls, *Algorithmica* 38 (2004) 161–177.
- [13] C. M. Shakarji, A. Clement, Reference algorithms for chebyshev and one-sided data fitting for coordinate metrology, *CIRP Annals - Manufacturing Technology* 53 (1) (2004) 439–442.
- [14] C. E. Kim, T. A. Anderson, Digital disks and a digital compactness measure, in: *Annual ACM Symposium on Theory of Computing*, 1984, pp. 117–124.
- [15] J. O'Rourke, S. R. Kosaraju, N. Meggido, Computing circular separability, *Discrete and Computational Geometry* 1 (1986) 105–113.
- [16] S. Fisk, Separating points sets by circles, and the recognition of digital disks, *IEEE Transactions on Pattern Analysis and Machine Intelligence* 8 (1986) 554–556.

- [17] V. A. Kovalevsky, New definition and fast recognition of digital straight segments and arcs, in: International Conference on Pattern Analysis and Machine Intelligence, 1990, pp. 31–34.
- [18] S. Pham, Digital circles with non-lattice point centres, *The Visual Computer* 9 (1992) 1–24.
- [19] M. Worring, A. W. M. Smeulders, Digitized circular arcs: characterization and parameter estimation, *IEEE Transactions on Pattern Analysis and Machine Intelligence* 17 (6) (1995) 554–556.
- [20] P. Damaschke, The linear time recognition of digital arcs, *Pattern Recognition Letters* 16 (1995) 543–548.
- [21] D. Coeurjolly, Y. Gérard, J.-P. Reveillès, L. Tougne, An elementary algorithm for digital arc segmentation, *Discrete Applied Mathematics* 139 (1-3) (2004) 31–50.
- [22] R. M. Haralick, A measure for circularity of digital figures, *IEEE Transactions on Systems, Man and Cybernetics* 4 (1974) 394–396.
- [23] U. Roy, X. Zhang, Establishment of a pair of concentric circles with the minimum radial separation for assessing roundness error, *Computer Aided Design* 24 (3) (1992) 161–168.
- [24] S. I. Gass, C. Witzgall, H. H. Harary, Fitting circles and spheres to coordinate measuring machine data, *The International Journal in Flexible Manufacturing Systems* 10 (1998) 5–25.
- [25] T. J. Rivlin, Approximation by circles, *Computing* 21 (1979) 93–104.
- [26] M. J. Bottema, Circularity of objects in images, in: International Conference on Acoustics, Speech, and Signal Processing, 2000, pp. 2247–2250.



- [27] D. Coeurjolly, R. Klette, A comparative evaluation of length estimators of digital curves, *IEEE Transactions on Pattern Analysis and Machine Intelligence* 26 (2004) 252–257.
- [28] I. Debled-Renesson, J.-P. Reveillès, A linear algorithm for segmentation of digital curves, *International Journal of Pattern Recognition and Artificial Intelligence* 9 (1995) 635–662.
- [29] R. O. Duda, P. E. Hart, Use of hough transformation to detect lines and curves in pictures, *Communications of the ACM* 15 (1) (1972) 11–15.
- [30] D. Luo, P. Smart, J. E. S. Macleod, Circular hough transform for roundness measurement of objects, *Pattern Recognition* 28 (11) (1995) 1745–1749.
- [31] S.-C. Pei, J.-H. Horng, Circular arc detection based on hough transform, *Pattern recognition letters* 16 (1995) 615–625.
- [32] U. M. Landau, Estimation of a circular arc centre and its radius, *Computer Vision, Graphics and Image Processing* 38 (1987) 317–326.
- [33] S. M. Thomas, Y. T. Chan, A simple approach to the estimation of circular arc centre and its radius, *Computer Vision, Graphics and Image Processing* 45 (1989) 362–370.
- [34] M. Berman, Large sample bias in least squares estimators of a circular arc centre and its radius, *Computer Vision, Graphics and Image Processing* 45 (1989) 126–128.
- [35] Z. Drezner, S. Steiner, G. O. Wesolowsky, On the circle closest to a set of point, *Computers and operations research* 29 (2002) 637–650.
- [36] T. Roussillon, I. Sivignon, L. Tougne, Test of circularity and measure of circularity for digital curves, in: *International Conference on Image Processing, Computer Vision and Pattern Recognition*, 2008, pp. 518–524.

- [37] N. Megiddo, Linear-time algorithms for linear programming in  $\mathbb{R}^3$  and related problems, *SIAM Journal on Computing* 12 (4) (1984) 759–776.
- [38] N. Megiddo, Linear programming in linear time when the dimension is fixed, *SIAM Journal on Computing* 31 (1984) 114–127.
- [39] R. Seidel, Small-dimensional linear programming and convex hulls made easy, *Discrete and Computational Geometry* 6 (1) (1991) 423–434.
- [40] F. P. Preparata, M. I. Shamos, *Computational geometry : an introduction*, Springer, 1985.
- [41] M. de Berg, M. van Kreveld, M. Overmars, O. Scharzkopf, *Computation geometry, algorithms and applications*, Springer, 2000.
- [42] G. H. Hardy, E. M. Wright, *An introduction to the theory of numbers*, Oxford science publications, 1978.
- [43] D. Aćketa, J. Zunić, On the maximal number of edges of convex digital polygons included into a  $m \times m$ -grid, *Journal of Combinatorial Theory, Series A* 69 (2) (1995) 358–368.
- [44] A. A. Melkman, On-line construction of the convex hull of simple polygon, *Information Processing Letters* 25 (1987) 11–12.
- [45] O. Devillers, F. P. Preparata, Culling a set of points for roundness or cylindricity evaluations, *International Journal of Computational Geometry and Applications* 13 (2003) 231–240.
- [46] T. Kanungo, R. M. Haralick, H. S. Baird, W. Stuezle, D. Madigan, A statistical, nonparametric methodology for document degradation model validation, *IEEE Transactions on Pattern Analysis and Machine Intelligence* 22 (2000) 1209–1223.

- [47] T. Hirata, A unified linear-time algorithm for computing distance maps, *Information Processing Letters* 58 (3) (1996) 129–133.
- [48] T. Roussillon, I. Sivignon, L. Tougne, Robust decomposition of a digital curve into convex and concave parts, in: *The 19th International Conference on Pattern Recognition (To appear)*, 2008.